The pure rotational spectrum of HPS ($\tilde{X}^1A'$): Chemical bonding in second-row elements

D. T. Halfen,[1] D. J. Clouthier,[2] L. M. Ziurys,[1] V. Lattanzi,[3] M. C. McCarthy,[3] P. Thaddeus,[3] and S. Thorwirth[4]

[1]*Departments of Chemistry and Astronomy, Arizona Radio Observatory, and Steward Observatory University of Arizona, Tucson, Arizona 85721, USA*
[2]*Department of Chemistry, University of Kentucky, Lexington, Kentucky 40506, USA*
[3]*Harvard-Smithsonian Center for Astrophysics, 60 Garden St., Cambridge, Massachusetts 02318, USA and School of Engineering & Applied Sciences, Harvard University, 29 Oxford St., Cambridge, Massachusetts 02318, USA*
[4]*I. Physikalisches Institut, Universität zu Köln, 50937 Köln, Germany, and Max-Planck-Institut für Radioastronomie, 53121 Bonn, Germany*

(Received 8 November 2010; accepted 14 February 2011; published online 1 April 2011)

The pure rotational spectrum of HPS, as well as its ^{34}S and D isotopologues, has been recorded at microwave, millimeter, and submillimeter wavelengths, the first observation of this molecule in the gas phase. The data were obtained using a combination of millimeter direct absorption, Fourier transform microwave (FTMW), and microwave–microwave double-resonance techniques, which cover the total frequency range from 15 to 419 GHz. Quantum chemical calculations at the B3LYP and CCSD(T) levels were also performed to aid in spectral identification. HPS was created in the direct absorption experiment from a mixture of elemental phosphorus, H_2S, and Ar carrier gas; DPS was produced by adding D_2. In the FTMW study, these species were generated in a pulsed discharge nozzle from PH_3 and H_2S or D_2S, diluted in neon. The spectra recorded for HPS and its isotopologues exhibit clear asymmetric top patterns indicating bent structures; phosphorus hyperfine splittings were also observed in HPS, but not DPS. Analysis of the data yielded rotation, centrifugal distortion, and phosphorus nuclear spin-rotation parameters for the individual species. The $r_m^{(1)}$ structure for HPS, calculated from the rotational constants, is r(H–P) = 1.438(1) Å, r(P–S) = 1.9320(1) Å, and θ(H–P–S) = 101.85(9)°. Empirically correcting for zero-point vibrational effects yields the geometry r_e(H–P) = 1.4321(2) Å, r_e(P–S) = 1.9287(1) Å, and θ_e(H–P–S) = 101.78(1)°, in close agreement with the $r_m^{(1)}$ structure. A small inertial defect was found for HPS indicating a relatively rigid molecule. Based on these data, the bonding in this species is best represented as H–P=S, similar to the first-row analog HNO, as well as HNS and HPO. Therefore, substitution of phosphorus and sulfur for nitrogen and oxygen does not result in a dramatic structural change. © *2011 American Institute of Physics*. [doi:10.1063/1.3562374]

I. INTRODUCTION

The bonding between second-row elements (i.e., Al through Cl) is a topic of considerable interest. The first-row elements, namely, carbon, oxygen, nitrogen, and even boron, are well-known to be able to form multiple bonds between themselves and/or each other.[1] However, experimental studies and theoretical work led to the consensus for sometime that multiple bonds with second-row elements could not exist,[2] the so-called "classical double bond rule." Since the 1960's, however, many species of this type have been discovered, including molecules with P=P and Si=Si double bonds.[2–5]

Even with the recent studies of silicon and phosphorus-bearing molecules, species with the P–S bond have remained elusive. Only FPS, ClPS, BrPS, and SPCN have been investigated, primarily in the infrared in an argon matrix.[6–9] The $\tilde{B}^2A' - \tilde{X}^2A'$ electronic transitions of F_2PS and Cl_2PS have also been recorded using laser-induced fluorescence (LIF) and single vibronic level emission spectroscopy.[10,11] Only one such species has been investigated at high spectral resolution, namely, FPS. Both pure rotational and high-resolution infrared spectra have been obtained for this molecule.[12]

Species with a P–S bond are also of astronomical interest. Six phosphorus-bearing molecules (HCP, CP, PN, CCP, PH_3, and PO) have thus far been detected in the circumstellar envelopes of old, evolved stars,[13–18] and PN has also been observed in dense molecular clouds.[19,20] Presumably other such species exist, perhaps some bearing a phosphorus-sulfur bond.

One obvious species containing a P–S bond is HPS, the second-row analog of HNO. Theoretical calculations have been performed for HPS using several *ab initio* methods at the HF, MP2, QCISD(T), and CCSD(T) levels.[21,22] The geometrical parameters, vibrational frequencies, and rotational constants of the ground state and triplet excited state have been estimated,[21,22] as well as the energy barrier between the HPS and HSP isomers.[22] HPS was first observed experimentally by neutralization–reionization mass spectrometry by Wong *et al.*

in 1992,[23] whose work indicated that this species, as well as HSP, were stable in the gas phase. The $\tilde{A}^1A'' - \tilde{X}^1A'$ electronic transitions of HPS and DPS have also been measured very recently using laser-induced fluorescence and single vibronic level emission spectroscopy.[24]

Here we report the first measurements of the pure rotational spectrum of HPS and its D and ^{34}S isotopologues from microwave to submillimeter wavelengths. Both direct absorption and Fourier transform methods were employed in this study, as well as high-level quantum-chemical calculations, which assisted in the experimental investigation. In this paper, these data, the corresponding spectroscopic constants, and the molecular structure are presented, along with a comparison of the bonding characteristics between the first- and second-row analogs.

II. EXPERIMENTAL

The pure rotational spectrum of HPS was first detected by direct absorption millimeter/submillimeter techniques using one of the instruments of the Ziurys group.[25] Briefly, this instrument consists of a frequency source, a free space gas cell, and a detector. The radiation source is a suite of Gunn oscillators combined with Schottky diode multipliers, covering a frequency range of 65–850 GHz. The glass reaction cell, which is chilled to −65 °C with methanol in a cooling jacket, contains two ring discharge electrodes in a longitudinal arrangement and is evacuated with a Roots-type blower pump. A liquid helium-cooled InSb hot electron bolometer is used as the detector. The radiation is propagated through the system using a series of Teflon lenses. Phase-sensitive detection is carried out by modulating the frequency source at a rate of 25 kHz, with 2*f* detection using a lock-in amplifier.

HPS and $HP^{34}S$ were created in the gas phase from a mixture of phosphorus vapor and H_2S with argon in the presence of an ac discharge. The ac discharge was operated at a power level of 150–200 W with an impedance of 600 Ω. The vapor was generated by heating solid elemental red phosphorus to ∼500 °C in a glass oven attached to the bottom of the cell, to which ∼5 mTorr of H_2S and 35 mTorr of Ar were added. To create DPS, 20 mTorr of D_2 was introduced to the reaction mixture. The ^{34}S isotopologue was recorded in natural abundance (^{32}S:^{34}S = 22.5:1). The H_2S–Ar mixture created a white-colored plasma in the cell; addition of D_2 altered the discharge color to red.

Transition frequencies were determined by measuring pairs of scans 5 MHz wide, one increasing in frequency and the other decreasing in frequency, to remove any systematic frequency shifts. For HPS, 2–4 such scans were necessary to achieve an adequate signal-to-noise ratio, while for DPS and $HP^{34}S$, 4–12 scans and 20–30 scans were needed, respectively. The experimental accuracy of the measurements is estimated to be ±50 kHz.

The microwave spectrum of HPS was measured using the Harvard Fourier transform microwave (FTMW) spectrometer, coupled with a supersonic molecular-beam discharge source; both have been described in detail elsewhere.[26] Measurements were also conducted using microwave–microwave double resonance techniques, as described in Ref. 27. Molecules are synthesized in the throat of a small supersonic nozzle by applying a low-current dc discharge to a short gas pulse created by a fast mechanical valve. The gas mixture normally consists of a precursor diluted to less than 1% in a neon buffer.

The mixture gases used for the FTMW search for HPS were optimized on a line of the PS radical at 26.4 GHz. The best conditions were found using a discharge potential of 1.2 kV in a mixture of H_2S and PH_3, heavily diluted in neon (∼0.1%), giving a total flow rate of about 20 cm^3 min^{-1} at standard temperature and pressure, with a stagnation pressure behind the valve of 2.5 kTorr and a 6 Hz nozzle pulse rate. Spectra of DPS were recorded by replacing H_2S with D_2S, and those of $HP^{34}S$ were observed in natural abundance. The spectra appear as Doppler doublets in the spectrum owing to the coaxial orientation of the fast-moving supersonic molecular beam relative to the microwave mode structure in the Fabry–Perot cavity. The experimental uncertainties of the observed transitions are 3 kHz for the FTMW experiments and 50 kHz for double resonance measurements.

III. QUANTUM-CHEMICAL CALCULATIONS

Previous theoretical studies of HPS predicted a bent molecule of $^1A'$ symmetry and a HSP ($^3A''$) geometric isomer lying approximately 67.8 kJ/mol above the HPS global minimum with an isomerization barrier of ∼106 kJ/mol.[21,28] In the present work, we used the GAUSSIAN 03 program suite to calculate the ground state structure and rotational constants of HPS prior to searches for the millimeter-wave spectrum.[29] Density functional theory with the Becke three parameter hybrid density functional and the Lee, Yang, and Parr correlation functional (B3LYP) was employed with Dunning's correlation-consistent quadruple-zeta basis set augmented by diffuse functions (aug-cc-pVQZ) to predict the molecular structure and vibrational frequencies.[30–33] A stable stationary point with a bent structure, r_e(PH) = 1.441 Å, r_e(PS) = 1.936 Å, and θ_e(HPS) = 102.1°, of singlet multiplicity and dipole moments of μ_a = 1.3 D and μ_b = 0.5 D were found. The rotational constants predicted by the calculations are A_e = 264,059 MHz, B_e = 8,330 MHz, and C_e = 8,075 MHz. These data were used as input to calculate the strongest millimeter-wave spectroscopic lines of HPS, and searches were carried out over a broad frequency range based on these rotational constants.

Additional quantum chemical calculations of HPS were performed using coupled-cluster theory at the CCSD(T) level.[34,35] These calculations were performed using the 2005 Mainz–Austin–Budapest version of ACESII and its successor CFOUR in its parallel incarnation.[36–38] Dunning's hierarchies of correlation-consistent polarized valence and polarized core valence basis sets were used throughout: in the frozen core (fc) approach, the *d*-augmented basis sets cc-pV(*X*+*d*)Z (*X* = T and Q) were used for the phosphorus and sulfur atoms and the cc-pV*X*Z basis sets for hydrogen.[30,33] The cc-pwCV*X*Z (*X* = T and Q) basis sets were used when considering all electrons in the correlation treatment.[39] Equilibrium geometries were obtained using analytic gradient techniques.[40] The best equilibrium structure of HPS has been calculated at the CCSD(T)/cc-pwCVQZ level

TABLE I. Selected rotational transition frequencies of HPS ($\tilde{X}^1A'$).

J′	K_a'	K_c'	F′	↔	J″	K_a''	K_c''	F″	ν_{obs} (MHz)	$\nu_{obs} - \nu_{calc}$ (MHz)
1	0	1	0.5	→	0	0	0	0.5	16490.334	−0.004
1	0	1	1.5	→	0	0	0	0.5	16490.374	0.001
2	0	2	1.5	→	1	0	1	1.5	32980.344	0.003
2	0	2	1.5	→	1	0	1	0.5	32980.374	−0.002
2	0	2	2.5	→	1	0	1	1.5	32980.401	0.002
15	1	15	[a]	←	14	1	14	[a]	245243.405	0.040
15	6	9	[a]	←	14	6	8	[a]	247070.605	−0.104
15	6	10	[a]	←	14	6	9	[a]	247070.605	−0.104
15	5	11	[a]	←	14	5	10	[a]	247138.792	−0.026
15	5	10	[a]	←	14	5	9	[a]	247138.792	−0.026
15	0	15	[a]	←	14	0	14	[a]	247167.696	0.021
15	4	12	[a]	←	14	4	11	[a]	247196.317	−0.051
15	4	11	[a]	←	14	4	10	[a]	247196.317	−0.051
15	2	14	[a]	←	14	2	13	[a]	247242.241	0.011
15	3	13	[a]	←	14	3	12	[a]	247245.541	0.043
15	3	12	[a]	←	14	3	11	[a]	247246.052	−0.075
15	2	13	[a]	←	14	2	12	[a]	247359.430	−0.015
15	1	14	[a]	←	14	1	13	[a]	249256.981	−0.011
19	1	19	[a]	←	18	1	18	[a]	310567.543	0.076
19	6	13	[a]	←	18	6	12	[a]	312904.891	−0.002
19	6	14	[a]	←	18	6	13	[a]	312904.891	−0.002
19	0	19	[a]	←	18	0	18	[a]	312935.155	−0.005
19	5	15	[a]	←	18	5	14	[a]	312992.322	−0.026
19	5	14	[a]	←	18	5	13	[a]	312992.322	−0.026
19	4	16	[a]	←	18	4	15	[a]	313067.505	0.001
19	4	15	[a]	←	18	4	14	[a]	313067.505	0.001
19	2	18	[a]	←	18	2	17	[a]	313104.677	−0.006
19	3	17	[a]	←	18	3	16	[a]	313134.403	0.030
19	3	16	[a]	←	18	3	15	[a]	313136.448	0.007
19	2	17	[a]	←	18	2	16	[a]	313342.747	−0.058
19	1	18	[a]	←	18	1	17	[a]	315646.791	[b]

[a]Hyperfine splittings collapsed.
[b]Blended line; not included in fit.

of theory previously shown to yield accurate equilibrium structures for molecules harboring second-row elements.[41,42] Harmonic and anharmonic force fields were calculated at the CCSD(T)/cc-pV(Q+*d*)Z level of theory using analytic second-derivative techniques followed by additional numerical differentiation to calculate the third and fourth derivatives needed for the anharmonic force field.[43–45] Theoretical ground state rotational constants are then obtainable from the equilibrium rotational constants [calculated at CCSD(T)/cc-pwCVQZ] and the zero-point vibrational contribution [calculated at CCSD(T)/cc-pV(Q+d)Z] according to

$$B_0^{qcc} = B_e^{qcc} - \frac{1}{2}\sum_i \alpha_i^{B,qcc}, \quad (1)$$

with similar equations for the A_0 and C_0 rotational constants. The force field calculations also yield the quartic centrifugal distortion constants. Nuclear quadrupole coupling constants for the deuterium species and nuclear spin-rotation constants for P were calculated at the CCSD(T)/cc-pwCVQZ level of theory employing perturbation-dependent basis functions for the latter.[46]

IV. RESULTS

The millimeter/submillimeter spectrum of HPS was identified by continuously scanning the region from 370 to 415 GHz. From the data, a pattern of multiple harmonically-repeating lines was identified that had the characteristic *a*-type pattern of a near prolate asymmetric top, with an effective rotational constant, $B_{eff} = (B+C)/2$, similar to the value predicted for HPS. Chemical tests were then performed which confirmed that these signals were due to both H_2S and phosphorus. In addition, strong lines of PS were recorded in the survey spectra. The carrier of the asymmetric top features was therefore assigned to HPS. No *b*-type transitions were evident in the data.

Four additional rotational transitions were subsequently detected using FTMW spectroscopy, including the two lowest $K_a = 1$ lines. Due to the high spectral resolution of the FTMW spectrometer, the spin-rotation splittings of the phosphorous nuclear spin ($I = 1/2$) were resolved for the $J_{Ka,Kc} = 1_{0,1} \rightarrow 0_{0,0}$ and $2_{0,2} \rightarrow 1_{0,1}$ transitions. Finally, double resonance microwave–microwave techniques were also used to extend the frequency range of the Harvard FTMW

TABLE II. Selected rotational transition frequencies of $HP^{34}S$ and DPS ($\tilde{X}^1A'$).

									$HP^{34}S$		DPS	
J'	$K_{a'}$	$K_{c'}$	F'	↔	J''	K_a''	K_c''	F''	ν_{obs} (MHz)	$\nu_{obs} - \nu_{calc}$ (MHz)	ν_{obs} (MHz)	$\nu_{obs} - \nu_{calc}$ (MHz)
1	0	1	0.5	→	0	0	0	0.5	16014.407	0.002	15831.384	−0.007
1	0	1	1.5	→	0	0	0	0.5	16014.440	0.000	15831.384	−0.007
2	0	2	1.5	→	1	0	1	1.5	32028.504	−0.002	31661.438	0.008
2	0	2	1.5	→	1	0	1	0.5	32028.542	0.002	31661.438	0.008
2	0	2	2.5	→	1	0	1	1.5	32028.562	−0.001	31661.438	0.008
22	1	22	[a]	←	21	1	21	[a]	349246.172	0.021	342480.486	−0.048
22	0	22	[a]	←	21	0	21	[a]	351778.693	0.049	345985.551	−0.072
22	2	21	[a]	←	21	2	20	[a]	352020.751	0.044	347708.824	−0.117
22	2	20	[a]	←	21	2	19	[a]	352348.892	−0.032	349813.309	0.016
22	1	21	[a]	←	21	1	20	[a]	354788.840	−0.024	352603.296	−0.189
26	1	26	[a]	←	25	1	25	[a]	412613.637	0.074	[b]	
26	0	26	[a]	←	25	0	25	[a]	415487.489	−0.033	407929.407	0.081
26	2	25	[a]	←	25	2	24	[a]	415900.712	0.068	410667.933	0.043
26	2	24	[a]	←	25	2	23	[a]	416440.400	−0.064	414021.226	−0.009
26	1	25	[a]	←	25	1	24	[a]	419153.805	0.040	416309.082	0.039

[a]Hyperfine splittings collapsed.
[b]Blended line; not included in fit.

spectrometer to above 41 GHz, enabling line frequencies of the $J_{Ka,Kc} = 3_{0,3} \rightarrow 2_{0,2}$ transition to be precisely determined (see Ref. 27 for details). The lowest two $K_a = 0$ rotational transitions of the ^{34}S and D substituted species were also recorded.

The millimeter/submillimeter search for $HP^{34}S$ and DPS was undertaken after the microwave detection and the CCSD(T) calculations were performed. Scaling the predicted rotational and centrifugal distortion constants for the ^{34}S isotopologue by the ratio of the experimental to theoretical values for HPS yielded predicted frequencies accurate to ±1–2 MHz. The millimeter/submillimeter spectrum of DPS was then found using a similar scaling technique, but the predicted frequencies were only accurate to ±10 MHz.

A sample of the rotational transitions measured for the main isotopologue of HPS is listed in Table I. The full dataset is available online.[47] Asymmetry components in the range $K_a = 0 - 6$ in twelve millimeter/submillimeter transitions in the range 228 – 415 GHz were recorded for this species. Only the asymmetry doublets of the $K_a = 0$, 1, 2, and 3 components were resolved. A total of 120 individual features were recorded. Three rotational transitions were measured in the microwave region, each exhibiting phosphorus hyperfine structure, resulting in a total of eight individual features.

Selected rotational transitions measured for $HP^{34}S$ and DPS are given in Table II. The rest of the data is available online.[47] Four transitions were measured in the millimeter region (342–419 GHz) for both isotopologues. Only the $K_a = 0$, 1, and 2 asymmetry components were observed due to the weaker intensities of these features. Furthermore, several lines of DPS were blended with other unknown features. Three transitions were recorded for $HP^{34}S$ and two for DPS in the microwave region. Only the $K_a = 0$ components could be identified in this case. Small splittings due to nuclear spin-rotation interactions were observed in the $K_a = 0$ components of the $J_{Ka,Kc} = 1_{0,1} \rightarrow 0_{0,0}$ and $2_{0,2} \rightarrow 1_{0,1}$ transitions of $HP^{34}S$, but could not be resolved in the $K_a = 1$ lines, nor in any of the DPS spectra.

A spectrum of the $J = 24 \leftarrow 23$ transition of HPS near 395 GHz, with numerous asymmetry features, is displayed in Fig. 1. The $K_a = 3$ lines have a small asymmetry splitting, as the figure shows, while that in the $K_a = 4$, 5, and 6 lines is collapsed. Only one component of the $K_a = 2$ doublet is seen

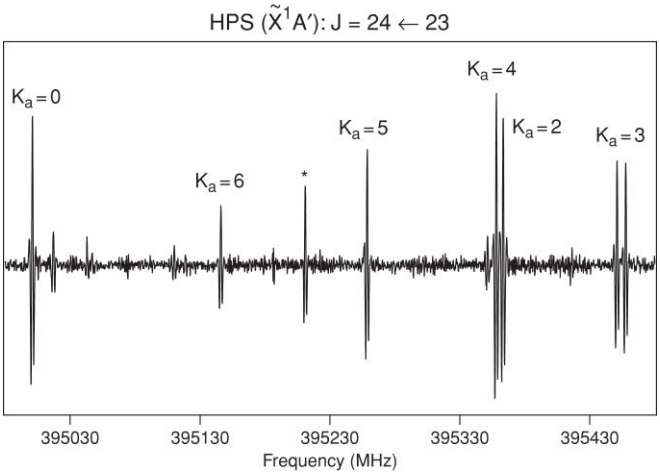

FIG. 1. Spectrum of the $J = 24 \leftarrow 23$ rotational transition of HPS ($\tilde{X}^1A'$) near 395 GHz, showing some of the $K_a = 0$, 2, 3, 4, 5, and 6 asymmetry components. These data clearly indicate that HPS is an asymmetric top and has a bent geometry. The $K_a = 2$ and 3 components are split by asymmetry doubling, with the $K_a = 3$ features closely spaced, while the other $K_a = 2$ component lies at higher frequency. A strong unknown feature is marked with an asterisk. This spectrum is a combination of five 110 MHz wide scans, each about 70 s in duration.

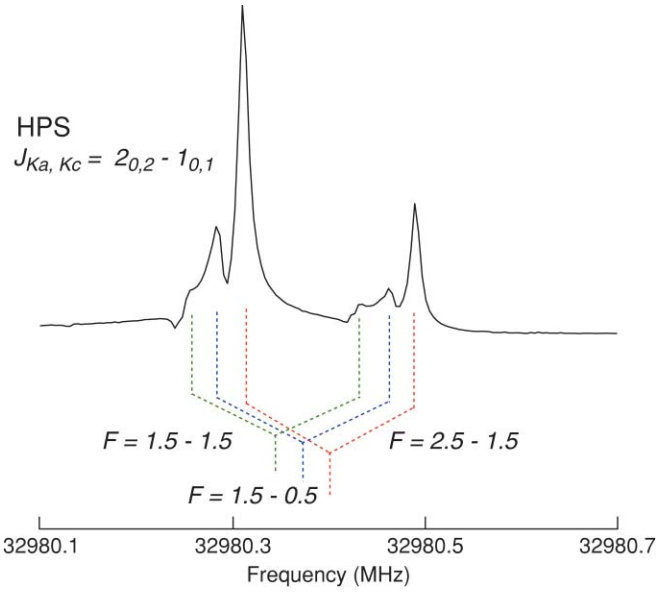

FIG. 2. Spectrum of the $J_{Ka,Kc} = 2_{0,2} \rightarrow 1_{0,1}$ transition of HPS near 33 GHz, which exhibits phosphorus nuclear spin-rotation hyperfine structure. Three hyperfine components are clearly visible, labeled by quantum number F. Each line is additionally split into Doppler doublets, indicated underneath the data. This spectrum was acquired in 35 s of integration.

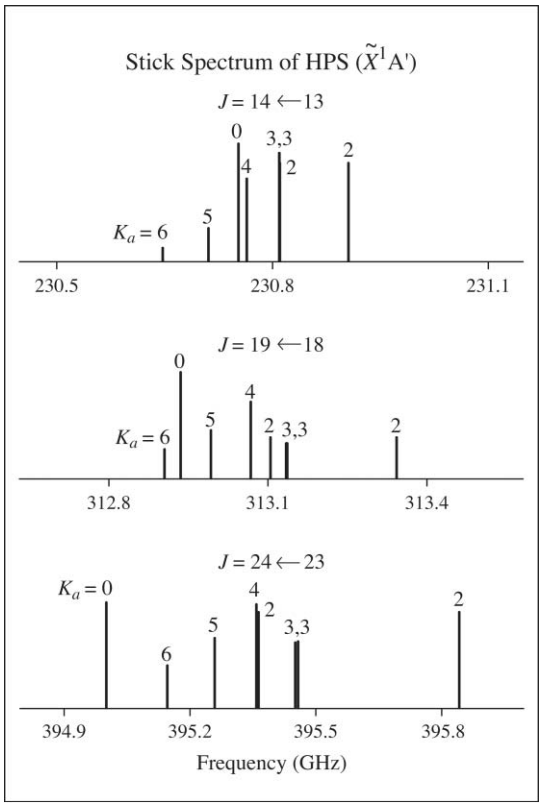

FIG. 3. Stick spectrum of the $K_a = 0$, 2, 3, 4, 5, and 6 asymmetry components of the $J = 14 \leftarrow 13$, $19 \leftarrow 18$, $24 \leftarrow 23$ rotational transitions of HPS ($\tilde{X}^1A'$) near 231, 313, and 395 GHz, respectively. The $K_a = 0$ and 2 asymmetry components shift significantly as a function of J, while the higher components $K_a = 4$, 5, and 6 are comparatively fixed in relative frequency.

in this frequency range. Other weaker, unidentified features are also apparent in the data.

A spectrum of the $J_{Ka,Kc} = 2_{0,2} \rightarrow 1_{0,1}$ transition of HPS near 33 GHz is displayed in Fig. 2. Here the three hyperfine components due to phosphorus nuclear spin-rotation interaction are apparent in the data. Each line is split into Doppler doublets indicated by lines underneath the spectrum.

An example of how the pattern of the asymmetry components changes as a function of J is shown in Fig. 3. Here a stick spectrum shows the $K_a = 0$, 2, 3, 4, 5, and 6 lines in the $J = 14 \leftarrow 13$, $19 \leftarrow 18$, and $24 \leftarrow 23$ transitions near 231, 313, and 395 GHz. The $K_a = 4$, 5, and 6 components do not shift significantly with respect to each other as a function of J, and the $K_a = 3$ component moves only slightly. In contrast, the $K_a = 0$ component shifts substantially, from close proximity to the $K_a = 4$ line at low J, to beyond the $K_a = 6$ line at high J. The $K_a = 2$ doublets also show increasing splitting as J increases.

V. ANALYSIS

The data for HPS, $HP^{34}S$, and DPS were individually analyzed with a Watson S-reduced Hamiltonian that included rotational, centrifugal distortion, and phosphorus nuclear spin-rotation interactions:[48]

$$\hat{H}_{eff} = \hat{H}_{rot} + \hat{H}_{cd} + \hat{H}_{nsr}. \quad (2)$$

The spectroscopic constants were determined using the nonlinear least squares fitting routine SPFIT.[49] In the fit, D_K for all three species was fixed to the value predicted by the CCSD(T) level of theory. In addition, two nuclear spin-rotation parameters arising from the phosphorus nucleus, C_{bb} and C_{cc}, were constrained to the ratio of the theoretical predictions, as they could not be independently determined due to the limited amount of data. C_{aa} for $HP^{34}S$ also had to be fixed to the value for HPS. The resulting parameters are given in Table III, which also lists the calculated values. As Table III shows, centrifugal distortion constants typically up to fourth-order were necessary for a good fit for the three species. The rms of the fits range from 38 to 67 kHz.

The rotational constants are in excellent agreement with the theoretical values at the CCSD(T) level, with the B and C parameters only differing by 0.05–0.07%, and A by 0.7%. The experimental centrifugal distortion constants are also in good agreement with the theoretical predictions. The hyperfine parameter C_{aa}, however, is about a factor of 2 less than the calculated value of 1.346 MHz.

VI. DISCUSSION

Several structures were calculated for HPS from the rotational constants using the nonlinear least squares routine STRFIT.[51] An r_0 geometry was determined directly from the moments of inertia, while an $r_m^{(1)}$ structure was also derived by a mass-dependent method developed by Watson.[52] A semiexperimental (empirical) structure was also calculated from the experimental rotational constants corrected for zero-point vibrational effects,[53] an approach used recently to determine equilibrium structures of related molecules such as

TABLE III. Spectroscopic constants for HPS, $HP^{34}S$, and DPS ($\tilde{X}^1A'$: v = 0).

	HPS			$HP^{34}S$		DPS	
Parameter [a]	Experiment	Theory[b]	Theory[c]	Experiment	Theory[b]	Experiment	Theory[b]
A_0	264,001(36)	265,808.909	264,059	263,961(91)	265,790.873	138,629.7(9.5)	139,246.636
B_0	8,379.1510(22)	8,373.766	8,330	8,133.578(17)	8,128.326	8,148.272(18)	8,142.849
C_0	8,111.2312(21)	8,107.055	8,075	7,880.870(17)	7,876.767	7,683.137(17)	7,679.463
ΔA_0		1,574.582			1,578.269		514.340
ΔB_0		18.258			17.561		17.323
ΔC_0		29.595			28.278		30.548
D_J	0.0052150(10)	0.00506		0.0049245(23)	0.00478	0.0045929(30)	0.00446
D_{JK}	0.20323(12)	0.199		0.19206(94)	0.188	0.1664(12)	0.162
D_K	19.6[d]	19.6		19.6[d]	19.6	5.56[d]	5.56
d_1	− 0.0001682(13)	− 0.000152		− 0.0001554(72)	− 0.000140	− 0.0002742(76)	− 0.000254
d_2	− 0.0000164(10)	− 0.0000129		− 0.0000146(16)	− 0.0000115	− 0.0000478(19)	− 0.0000392
H_{KJ}	$2.49(36) \times 10^{-5}$						
C_{aa}	0.701(45)	1.346		0.701[d]			
C_{bb}	0.0371(45)[e]	0.0476		0.0372(69)[e]			
C_{cc}	0.0091(11)[e]	0.0116		0.0091(17)[e]			
rms	0.038			0.040		0.067	

[a]In MHz.
[b]Structure: CCSD(T)/cc-pwCVQZ level, force field: CCSD(T)/cc-pV(Q+d)Z level.
[c]Equilibrium constants at the B3LYP/aug-cc-pVTZ level.
[d]Held fixed.
[e]Constrained to the ratio of the theoretical values.

HPSi, H_2SiS, and Si_2S.[50,54,55] This empirical structure was established by adding the theoretical vibrational corrections ΔB_0 and ΔC_0 (Table III) to the experimentally determined rotational constants B_0 and C_0 (Table III), i.e., $B_e = B_0 + \Delta B_0$. A least-squares fit of the HPS structural parameters was then carried out using the six I_b and I_c equilibrium moments of inertia obtained from the corresponding empirical B_e and C_e constants adopting equal weights for all isotopologues.

The structures generated for HPS are listed in Table IV, along with those predicted by the quantum-chemical calculations described here, as well as several other theoretical geometries.[21,22] Figure 4 shows the empirically established r_e^{emp} structure. Also given in Table IV are the bond lengths and angles of several other species related to HPS.[12,22,56–58] As can be seen from the table, the H–P bond length in HPS (r_e^{emp} = 1.4321(2) Å) is very similar in value to that found for PH (r_0 = 1.4328(1) Å) and PH_3 (r_e = 1.4115(6) Å),[56,57] and the calculated value for HPSH (r_e = 1.416 Å: QCISD /6–311++G(*d*,*p*).[22] This accord indicates that there is a H–P single bond in HPS. The PS bond length of this species (r_e^{emp} = 1.9287(1) Å) compares closely to that found for PS (r_0 = 1.9003(1) Å) and FPS (r_e^{emp} = 1.8886(4) Å). The PS bond length in HPSH is predicted to be longer (r_e = 2.120(1) Å), likely reflecting a single P–S bond. The significantly shorter P–S bond distance for HPS relative to HPSH suggests a P=S double bond. Thus, the bonding of this molecule is best represented as H–P=S.

The H–P–S bond angle was determined to be θ = 101.78(1°) from the r_e^{emp} method. This value lies between the HPS angle calculated for HPSH (91.6°) and the

TABLE IV. Structural parameters of HPS and related molecules.

Molecule	*r*(H–P) (Å)	*r*(P–S) (Å)	θ (XPS) (deg)	Method[a]	Ref.
HPS	1.444(5)	1.931(1)	101.6(5)	r_0	This work
	1.438(1)	1.9320(1)	101.85(9)	$r_m^{(1)}$ [b]	This work
	1.4321(2)	1.9287(1)	101.78(1)	r_e^{emp}	This work
	1.4436	1.9423	101.9251	r_e, *ab initio* B3LYP/cc-pVTZ	This work
	1.4303	1.9293	101.84	r_e, *ab initio* CCSD(T)/cc-pwCVQZ	This work
	1.425	1.949	102.3	r_e, *ab initio* MP2/6–31G(*d*,*p*)	21
	1.430	1.949	101.95	r_e, *ab initio* QCISD/6–311++G(*d*,*p*)	22
P−H	1.4328(1)			r_0, MMW	56
PH_3	1.420(1)			r_0, MMW	57
	1.4115(6)			r_e, MMW	57
P=S		1.9003(1)		r_0, MMW	58
H−P−S−H	1.416	2.120	91.6	r_e, *ab initio* QCISD/6–311++G(*d*,*p*)	22
F−P=S		1.8886(4)	109.28(2)	r_e^{emp}, IR, MMW, *ab initio*	12

[a]MMW = millimeter wave.
[b]$c_b = -0.0113(8)$.

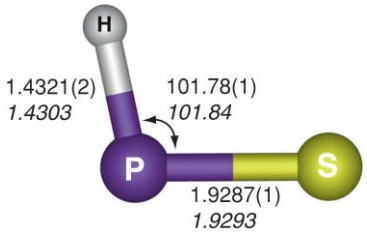

FIG. 4. Semiexperimental equilibrium structure of HPS (bond lengths in Angstroms and angle in degrees) and calculated structure obtained at the CCSD(T)/cc-pwCVQZ level of theory (in italics).

experimental bond angle in FPS (109.28°). The near 90° angle in HPSH likely reflects purely *p* orbital bonding. In FPS, the larger bond angle may result from a certain degree of sp^2 hybridization on the phosphorus atom.

The structure of HPS can also be compared to its singly- and doubly-substituted first-row analogs HNO, HNS, and HPO. The geometries of these four species are listed in Table V.[59,60] The bond lengths and angle of HNO were calculated from the rotational constants of HNO and DNO using STRFIT,[51] as the structure was not given in Ref. 59. The geometry of HNS had to be calculated at the B3LYP/aug-cc-pVTZ level because it has not been studied experimentally. As can be seen from the table, the H–P bond lengths of HPO and HPS are very close in value at 1.43 – 1.47 Å. The heavy atom bond length, in contrast, increases on substitution of a second-row element, from 1.21 to 1.57 Å for N–O to N–S, and 1.48 to 1.93 Å for P–O to P–S and is longest in HPS. These changes likely reflect the larger atomic radii of the second-row elements.

Comparison of the bond angles among these species perhaps presents more chemical insight. The bond angle for the first row molecules, HNO and HNS, is 108–110°, while it decreases to ∼105° for HPO and ∼102° for HPS. This trend suggests that the bonding is basically similar in all molecules with a double bond between the heavy atoms, i.e., N = O, N=S, P=O, and P=S. The bond angle in all cases reflects sp^2 hybridization, altered by the presence of lone pair electrons, which closes the angle somewhat relative to 120°. This effect is also seen in vinyl anion (CH_2=CH^-), a similar species with a C=C–H moiety that has a bond angle of ∼108.5°.[61] The bond angle becomes even smaller, however, for HPO and HPS, likely a result of increased *p* orbital contribution of phosphorus, relative to nitrogen. If the bonding were purely due to *p* orbitals, an angle of ∼90° would be expected, as seen in SrSH and BaSH.[62,63]

The small difference in the HPO and HPS bond angles is also notable. This disparity, ∼105° for HPO and ∼102° for HPS, can be explained by a small contribution from the ionic resonance form, linear H–P^+≡O^-, to H–P=O. The electronegativity of oxygen is greater than that of sulfur (χ(O) = 3.4, χ(S) = 2.6),[64] and thus this structure is more likely to play a role in HPO as opposed to HPS. Because this resonance form is linear it would slightly increase the H–P–O bond angle relative to HPS, as observed.

The zero-point inertial defects, Δ_0, for HPS, $HP^{34}S$, and DPS were calculated to be 0.078 amuÅ^2 for HPS and $HP^{34}S$ and 0.109 amuÅ^2 for DPS, based on the rotational constants, A_0, B_0, and C_0. For closed-shell, planar molecules, this parameter has contributions from harmonic and Coriolis terms of vibration–rotation interactions:[65]

$$\Delta_0 = \Delta_0^{\text{harm}} + \Delta_0^{\text{Cor}}. \tag{3}$$

The Coriolis interaction is generally negligible for small molecules.[65] Therefore, the harmonic term is the dominant contributor to Δ_0 in HPS. This parameter can also be calculated from the centrifugal distortion constants D_J, D_{JK}, d_1, and d_2.[65] It was determined to be 0.084 amuÅ^2 for HPS, 0.085 amuÅ^2 for $HP^{34}S$, and 0.114 amuÅ^2 for DPS. These values are slightly larger than the experimentally determined values of Δ_0, and such differences likely reflect a small, negative Coriolis contribution. Using the empirical equilibrium rotational constants, the inertial defect was calculated to be −0.006 amuÅ^2 for all three species of HPS, i.e., essentially zero. The vibrational contributions can therefore be effectively removed by applying the calculated zero-point corrections. Using their experimentally derived rotational constants, the inertial defects of HNO, DNO, HPO, and DPO were calculated to be 0.048 amuÅ^2, 0.063 amuÅ^2, 0.079 amuÅ^2, and 0.105 amuÅ^2, respectively. All of these values are small and positive; hence, these molecules are all relatively rigid species, supporting the notion of a double bond between the heavy heteroatoms.

To first order, the nuclear spin-rotation hyperfine interaction in HPS results from the coupling of the phosphorus nuclear magnetic moment (μ_I = 1.13160(3) μ_N) (Ref. 66) with the magnetic field generated by the rotation of the molecule about the three principle axes. This field is typically weak and usually results in small values for the C_{aa}, C_{bb}, and C_{cc} hyperfine parameters. A second-order correction is also possible, arising from nuclear spin-orbit coupling with nearby electronic states. In this case, the orbiting electrons create the magnetic field, which generates a much stronger coupling. Considering the effects of the nearest excited state A^1A'', this interaction is expressed as[67]

$$C_{ii} = \frac{4B_{ii}a_{XA}\,|\langle X|\,L_i\,|A\rangle|^2}{E_A - E_X}. \tag{4}$$

Here B_{ii} are the ground state rotational constants, a_{XA} is the off-diagonal nuclear spin-orbit interaction constant, L_i is the *i* component of the orbital angular momentum, and E_A and E_X are the energies of the excited and ground states. The excited state does not have to have orbital angular momentum as long

TABLE V. Structural parameters of HPS and Nitrogen and/or Oxygen Analogs.

Molecule	*r*(H-X) (Å)	*r*(X-Y) (Å)	θ (HXY) (deg)	Method	Ref.
HNO	1.063(2)	1.2123(5)	108.42(14)	$r_m^{(1)}$[a]	59
HNS	1.028	1.570	109.7	r_e[b]	This work
HPO	1.473(7)	1.4843(9)	104.57(16)	r_z	60
HPS	1.4321(2)	1.9287(1)	101.78(1)	r_e^{emp}	This work

[a]Calculated from constants from Ref. 59.
[b]Calculated at the B3LYP/aug-cc-pVTZ level.

as it correlates to a state that does in the linear limit. For HPS, the likely state involved is A^1A'', which correlates with a $^1\Pi_i$ state in the linear limit.[24] As this expression suggests, the nuclear spin-rotation parameters should be proportional to the respective rotational constants, if the second-order effect dominates. The C_{aa}, C_{bb}, and C_{cc} constants for HPS have the values of 0.701 MHz, 0.0371, and 0.0091 MHz, respectively, which closely correlate with the rotational constants A_0 = 264,001(36), B_0 = 8,379.1510(22), and C_0 = 8,111.2313(21). The dominance of the second-order term explains why the phosphorus hyperfine splitting was not resolved in DPS. This splitting likely reflects the much smaller value of A_0 relative to HPS: 264,001(36) versus 138,629.7(9.5) MHz.

VII. CONCLUSION

High-resolution gas-phase studies of simple molecules with second-row elements can produce useful chemical insights into this class of species. This combined microwave and millimeter-wave investigation of HPS has shown that this molecule is bent, with an angle near 102°. Furthermore, the molecule has a P=S double bond and a P–H single bond. Consequently, it appears to mimic the structure of HNO, as well as HPO and HNS. The geometry results from sp^2 hybridization at the phosphorus atom with distortion from the lone pair electrons, as well as some contribution from the *p* orbitals. The *p* orbital influence is more important in phosphorus and sulfur than in nitrogen and oxygen. A small inertial defect exists in HPS, indicating that this species is quite rigid. This rigidity is also reflected in the lack of higher-order centrifugal distortion constants in the spectral analysis. Additional studies of simple species with second-row elements are clearly needed to further elucidate their chemistry.

ACKNOWLEDGMENTS

The work here was supported by the NSF Grant No. AST 09–06534 and NASA Exobiology Grant No. NNX10AR83G. D.J.C. also acknowledges NSF support. The work in Cambridge was supported by NSF Grant No. CHE 07–01204 and NASA Grant No. NNX08AE05G. S.T. is grateful to the Deutsche Forschungsgemeinschaft for a research Grant No. (TH 1301/3–1).

[1] R. T. Morrison and R. N. Boyd, *Organic Chemistry*, 6th ed. (Prentice-Hall, Englewood Cliffs, 1992).
[2] P. Jutzi, Angew. Chem., Int. Ed. **14**, 232 (1975).
[3] L. E. Gusel'nikov and N. S. Nametkin, Chem. Rev. **79**, 529 (1979).
[4] A. H. Cowley, Polyhedron **3**, 389 (1984).
[5] P. P. Power, Chem. Rev. **99**, 3463 (1999).
[6] H. Schnöckel and S. Schunck, Z. Anorg. Allg. Chem. **552**, 155 (1987).
[7] H. Schnöckel and S. Schunck, Z. Anorg. Allg. Chem. **552**, 163 (1987).
[8] M. Binnewies and H. Schnöckel, Chem. Rev. **90**, 321 (1990).
[9] A. W. Allaf and M. N. Odeh, Spectrochim. Acta, Part A **62**, 282 (2005).
[10] J. Yang, D. J. Clouthier, and R. Tarroni, J. Chem. Phys. **131**, 224311 (2009).
[11] J. Yang, X. Zhang, D. J. Clouthier, and R. Tarroni, J. Chem. Phys. **131**, 204307 (2009).
[12] H. Beckers, M. Bogey, J. Breidung, H. Bürger, J. Demaison, P. Dréan, P. Paplewski, W. Thiel, and A. Walters, J. Mol. Spectrosc. **210**, 213 (2001).
[13] M. Agúndez, J. Cernicharo, and M. Guélin, Astrophys. J. **662**, L91 (2007).
[14] M. Guélin, J. Cernicharo, G. Paubert, and B. E. Turner, Astron. Astrophys. **230**, L9 (1990).
[15] S. N. Milam, D. T. Halfen, E. D. Tenenbaum, A. J. Apponi, N. J. Woolf, and L. M. Ziurys, Astrophys. J. **684**, 618 (2008).
[16] D. T. Halfen, D. J. Clouthier, and L. M. Ziurys, Astrophys. J. **677**, L101 (2008).
[17] E. D. Tenenbaum and L. M. Ziurys, Astrophys. J. **680**, L121 (2008).
[18] E. D. Tenenbaum, N. J. Woolf, and L. M. Ziurys, Astrophys. J. **666**, L29 (2007).
[19] L. M. Ziurys, Astrophys. J. **321**, L81 (1987).
[20] B. E. Turner, Astrophys. J. **321**, L75 (1987).
[21] M. T. Nguyen, Chem. Phys. **117**, 91 (1987).
[22] R. B. Viana and A. S. Pimentel, J. Chem. Phys. **127**, 204306 (2007).
[23] T. Wong, J. K. Terlouw, H. Keck, W. Kuchen, and P. Tommes, J. Am. Chem. Soc. **114**, 8208 (1992).
[24] R. A. Grimminger, J. Wei, B. Ellis, D. J. Clouthier, Z. Wang, and T. Sears, 64th Int. Sym. Mol. Spectrosc. TJ05 (2009).
[25] C. Savage and L. M. Ziurys, Rev. Sci. Instrum. **76**, 043106 (2005).
[26] M. C. McCarthy, W. Chen, M. J. Travers, and P. Thaddeus, Astrophys. J., Suppl. **129**, 611 (2000).
[27] V. Lattanzi, P. Thaddeus, M. C. McCarthy, and S. Thorwirth, J. Chem. Phys. **133**, 194305 (2010).
[28] W. N. Wang, W. L. Wang, Q. Luo, and Q. S. Li, Chem. Phys. Lett. **415**, 370 (2005).
[29] M. J. Frisch, *et al.* GAUSSIAN, 03, Revision C.02 Gaussian, Inc., Wallingford, CT, 2004.
[30] T. H. Dunning, J. Chem. Phys. **90**, 1007 (1989).
[31] A. D. Becke, J. Chem. Phys. **98**, 5648 (1993).
[32] C. Lee, W. Yang, and R. G. Parr, Phy. Rev. B **37**, 785 (1988).
[33] T. H. Dunning, K. A. Peterson, and A. K. Wilson, J. Chem. Phys. **114**, 9244 (2001).
[34] J. Gauss, in *Encyclopedia of Computational Chemistry*, edited by P. V. R. Schleyer, N. L. Allinger, T. Clark, J. Gasteiger, P. A. Kollmann, H. F. Schaefer, and P. R. Schreiner (Wiley, Chichester, 1998), pp. 615.
[35] K. Raghavachari, G. W. Trucks, J. A. Pople, and M. Head-Gordon, Chem. Phys. Lett. **157**, 479 (1989).
[36] ACESII, a quantum-chemical program written by J. F. Stanton, J. Gauss, J. D. Watts, P. G. Szalay, and R. J. Bartlett (2005), with contributions from A. A. Auer, D. E. Bernholdt, O. Christiansen, M. E. Harding, M. Heckert, O. Heun, C. Huber, D. Jonsson, J. Jusélius, W. J. Lauderdale, T. Metzroth, C. Michauk, D. R. Price, K. Ruud, F. Schi_mann, A. Tajti, M. E. Varner, J. Vázquez and the integral packages: MOLECULE (J. Almlöf and P. R. Taylor), props (P. R. Taylor), and ABACUS (T. Helgaker, H. J. Aa. Jensen, P. Jørgensen, and J. Olsen). Current version see http://www.aces2.de.
[37] CFOUR, a quantum chemical program package written by J. F. Stanton, J. Gauss, M. E. Harding, P. G. Szalay with contributions from A. A. Auer, R. J. Bartlett, U. Benedikt, C. Berger, D. E. Bernholdt, O. Christiansen, M. Heckert, O. Heun, C. Huber, D. Jonsson, J. Jusélius, K. Klein, W. J. Lauderdale, D. Matthews, T. Metzroth, D. P. O'Neill, D. R. Price, E. Prochnow, K. Ruud, F. Schiffmann, S. Stopkowicz, M. E. Varner, J. Vázquez, F. Wang, J. D. Watts and the integral packages MOLECULE (J. Almlöf and P. R. Taylor), PROPS (P. R. Taylor), ABACUS (T. Helgaker, H. J. Aa. Jensen, P. Jørgensen, and J. Olsen), and ECP routines by A. V. Mitin and C. van Wüllen. For the current version, see http://www.cfour.de.
[38] M. E. Harding, T. Metzroth, J. Gauss, and A. A. Auer, J. Chem. Theory Comput. **4**, 64 (2008).
[39] K. A. Peterson and T. H. Dunning, J. Chem. Phys. **117**, 10548 (2002).
[40] J. D. Watts, J. Gauss, and R. J. Bartlett, Chem. Phys. Lett. **200**, 1 (1992).
[41] S. Coriani, D. Marcheson, J. Gauss, C. Hättig, T. Helgaker, and P. Jørgensen, J. Chem. Phys. **123**, 184107 (2005).
[42] S. Thorwirth and M. E. Harding, J. Chem. Phys. **130**, 214303 (2009).
[43] J. Gauss and J. F. Stanton, Chem. Phys. Lett. **276**, 70 (1997).
[44] J. F. Stanton and J. Gauss, Int. Rev. Phys. Chem. **19**, 61 (2000).
[45] J. F. Stanton, C. L. Lopreore, and J. Gauss, J. Chem. Phys. **108**, 7190 (1998).
[46] J. Gauss, K. Ruud, and T. Helgalker, J. Chem. Phys. **105**, 2804 (1996).
[47] See supplementary material at http://dx.doi.org/10.1063/1.3562374 for a complete list of the measured transition frequencies of HPS, $HP^{34}S$, and DPS.
[48] J. K. G. Watson, *Vibrational Spectra and Structure*, edited by J. R. Durig (Elsevier, Amsterdam, 1977), p. 1.

[49]H. M. Pickett, J. Mol. Spectrosc. **148**, 371 (1991).
[50]V. Lattanzi, S. Thorwirth, D. T. Halfen, L. A. Mück, L. M. Ziurys, P. Thaddeus, J. Gauss, and M. C. McCarthy, Angew. Chem., Int. Ed. **49**, 5661 (2010).
[51]Z. Kisiel, J. Mol. Spectrosc. **218**, 58 (2003).
[52]J. K. G. Watson, A. Roytburg, and W. Ulrich, J. Mol. Spectrosc. **196**, 102 (1999).
[53]C. Puzzarini, J. F. Stanton, and J. Gauss, Int. Rev. Phys. Chem. **29**, 273 (2010).
[54]S. Thorwirth, J. Gauss, M. C. McCarthy, F. Shindo, and P. Thaddeus, Chem. Commum. (Cambridge) 5292 (2008).
[55]M. C. McCarthy, C. A. Gottlieb, P. Thaddeus, S. Thorwirth, and J. Gauss, J. Chem. Phys. **134**, 034306 (2011).
[56]E. Klisch, H. Klein, G. Winnewisser, and E. Herbst, Z. Naturforsch. **53a**, 733 (1998).
[57]D. A. Helms and W. Gordy, J. Mol. Spectosc. **66**, 206 (1977).
[58]M. Ohishi, S. Yamamoto, S. Saito, K. Kawaguchi, H. Suzuki, N. Kaifu, S.-I. Ishikawa, S. Takano, T. Tsuji, and W. Unno, Astrophys. J. **329**, 511 (1988).
[59]K. V. L. N. Sastry, P. Helminger, G. M. Plummer, E. Herbst, and F. C. De Lucia, Astrophys. J. **55**, 563 (1984).
[60]H. Ozeki and S. Saito, J. Mol. Spectrosc. **219**, 305 (2003).
[61]A. C. Simmonett, S. E. Wheeler, and H. F. Schafer, III, J. Phys. Chem. A **108**, 1608 (2004).
[62]D. T. Halfen, A. J. Apponi, J. M. Thompsen, and L. M. Ziurys, J. Chem. Phys. **115**, 11131 (2000).
[63]A. Janczyk and L. M. Ziurys, J. Chem. Phys. **119**, 10702 (2003).
[64]C. H. Suresh and N. Koga, J. Am. Chem. Soc. **124**, 1790 (2002).
[65]J. K. G. Watson, J. Chem. Phys. **98**, 5302 (1993).
[66]N. J. Stone, A. Data Nucl. Data Tables **90**, 75 (2005).
[67]C. H. Townes and A. L. Schawlow, *Microwave Spectroscopy* (Dover, New York, 1975).